

Article

# Toward Understanding of the Effect of Nucleation Temperature on Porous Structure of Micro-Mesoporous Composite Molecular Sieves and Related Crystallization Mechanism

Chunwei Shi <sup>1,2,\*</sup>, Jingjing Liu <sup>1</sup>, Wenyuan Wu <sup>3</sup>, Xue Bian <sup>3</sup>, Ping Chen <sup>1</sup>, Zhanxu Yang <sup>1</sup> and Chuantao Lu <sup>4</sup>

<sup>1</sup> College of Chemistry, Chemical Engineering and Environmental Engineering, Liaoning Shihua University, Funshun 113001, China; LJJ18340356115@126.com (J.L.); chunchun-516@126.com (P.C.); zhanxuy@126.com (Z.Y.)

<sup>2</sup> Administration Center of the Yellow River Delta Sustainable Development Institute of Shandong Province, Dongying 257001, China

<sup>3</sup> School of Materials and Metallurgy, Northeastern University, Shenyang 110819, China; LJJ19970924@163.com (W.W.); ljandthd@126.com (X.B.)

<sup>4</sup> PetroChina Fushun Petrochemical Company, Fushun 113001, China; luct-sc@petrochina.com.cn

\* Correspondence: chunweishilnpu@126.com

Received: 24 August 2019; Accepted: 12 September 2019; Published: 17 September 2019



**Abstract:** Although micro-mesoporous composite molecular sieves have received significant attention due to their desirable properties, they still lack systematic studies on their crystallization process to achieve controllable synthesis of composite molecular sieves. In this study, a series of Y/SBA-15 micro-mesoporous composite molecular sieves with different porous structures were synthesized by tuning nucleation temperature, based on epitaxial growth on the outer surface of the Y-type crystal particle. All composite molecular sieves were characterized by X-ray diffraction (XRD), scanning electron microscope (SEM), and transmission electron microscope (TEM). Moreover, the effect of nucleation temperature on the structure of composite molecular sieves was investigated, while the crystallization mechanism was also explored. Furthermore, the performance of the molecular sieves on isomerization of *n*-pentane was investigated, the results suggested that the isomerization selectivity was positively correlated with regularity degree of the mesoporous porous structure, where the highest isomerization reached 95.81%. This work suggests that nucleation temperature plays a key role in structures of micro-mesoporous composite molecular sieves, providing a solid basis for the further development of functional composite molecular sieves.

**Keywords:** core-shell structure; composite molecular sieve; nucleation stage; nucleation temperature; growth mechanism; isomerization

## 1. Introduction

Micro-mesoporous composite molecular sieves have been widely used in the petrochemical field, due to the simultaneous presence of a microporous and mesoporous structure. Among them, micro-mesoporous composite molecular sieves containing a core-shell structure have received significant attention recently; in these sieves, the outer surface of the active core (e.g., ZSM-5) can be modified with a pure silicon molecular sieve (e.g., Silicalite 1 or SBA-15) to adjust the surface acidity to prevent adverse events, while retaining the acidity and porous size of their inner surface. Up to now, there have been mainly two methods to prepare these core-shell structured composite

molecular sieves: the isomorphic growth method and the epitaxial growth method. In particular, the epitaxial growth enables the growth of another structure or composition on the outer surface of a core, forming a composite core-shell structure with some particular properties, such as catalytic activity [1,2].

Significant attention has been paid to studying the forming mechanism of core-shell structured composite molecular sieves, due to their properties heavily depending on their structure [3–9]. Especially, the effect of synthesis conditions including temperature and time on multiple-layer pore structure have been extensively investigated. Many studies have been done to investigate the effect of these experimental parameters on the structure of the composite molecular sieves based on the epitaxial method. Most of them focused on experimental parameters' effect on the crystallization process. For example, Wang et al. [3] systematically investigated the influence of crystallization temperature and time on the formation of shell and core, obtaining high density and coverage shell, this core-shell structured molecular sieve displays rhombic crystal morphology with a complete MFI/CHA composite core-shell structure. Our team also utilized the cation-exchange effect to grow the template agent on the surface of the Y microporous molecular sieve [10], and investigated the crystallization mechanism of Y/SBA-15 composite molecular sieve. We found that the replacement of aluminum with silicon in the four-membered ring can reduce the stability of the unit cell since the size of the silicon atom is smaller than aluminum's. This further leads to irregular contraction of the unit cell. Thus, reduced stability plays a guiding role.

Recently, the nucleation stage of single molecular sieves has been extensively studied [11–13]. Yang et al [14] found that the introduction of iron (Fe) could promote the crystal grain formation of Eu-1 molecular sieve, and further investigated the relationship between nucleation rate and crystal growth rate of Fe. Xing et al [15] reviewed recent advances in pre-crystallization phase formation during the crystallization of SAPO-34 molecular sieve and the nucleation during the induction period, concluding that an unstable layered pre-crystallization phase structure was first formed during the crystallization process, and further developed into the orderly crystal lattice arrangement. It is deduced that crystallization kinetics control the nucleation and growth rate of crystals, of which temperature is the key factor. However, although nucleation stage plays a key role in the porous structure of composite molecular sieves, there were few reports studying the nucleation stage of composite molecular sieves. For example, Hammed et al [16] reported a SuZSM-5 composite molecular sieve, and investigated the effect of crystallization conditions (e.g., pH, temperature, time) on its loading capacity to methylene blue, which increased the maximum loading capacity from 20.68 mg/g to 86.70 mg/g. Therefore, it is necessary to unmask the nucleation mechanism of composite molecular sieves, due to its significant role in the controllable preparation of composite molecular sieves. Taken together, the prepared molecular sieves displayed microporous and mesoporous structures, which are significantly different from hybrid materials. Thus, these verify that they are the micro-mesoporous composite molecular sieves. In addition, temperature plays an important role in porous structures of the molecular sieves. Low temperature can result in bad porous structure and connectivity.

In this work, we applied the epitaxial growth to prepare composite molecular sieves, and investigated the effect of temperature on porous structure. A range of techniques including XRD, SEM, and TEM were used to characterize the morphology and porous structure of composite molecular sieves, studying the effect of nucleation temperature on the porous structure. Furthermore, using *n*-pentane as a template agent, the performance of these composite molecular sieves on hydroisomerization of *n*-pentane were investigated by a continuous-flow high-pressure microreactor-chromatography apparatus.

## 2. Results and Discussion

### 2.1. Characterization of YSV Micro-Mesoporous Composite Molecular Sieve

We first investigated the morphology and structure of the prepared YSV composite molecular sieve; during the reaction the temperature at the nucleation stage was 10 °C. As shown in Figure 1,

the simultaneous presence of microporous and mesoporous characteristic structures was observed (Figure 1a,b), confirming the generation of micro-mesoporous composite molecular sieves under 10 °C of the nucleation temperature. As seen from Figure 1c–e, the samples displayed foam or cotton-like morphology. The cores showed Y-type microporous porous structure, while the shells showed cotton-like SBA-15 mesoporous porous structure around the cores. Moreover, the boundary between microporous and mesoporous was clearly observed.

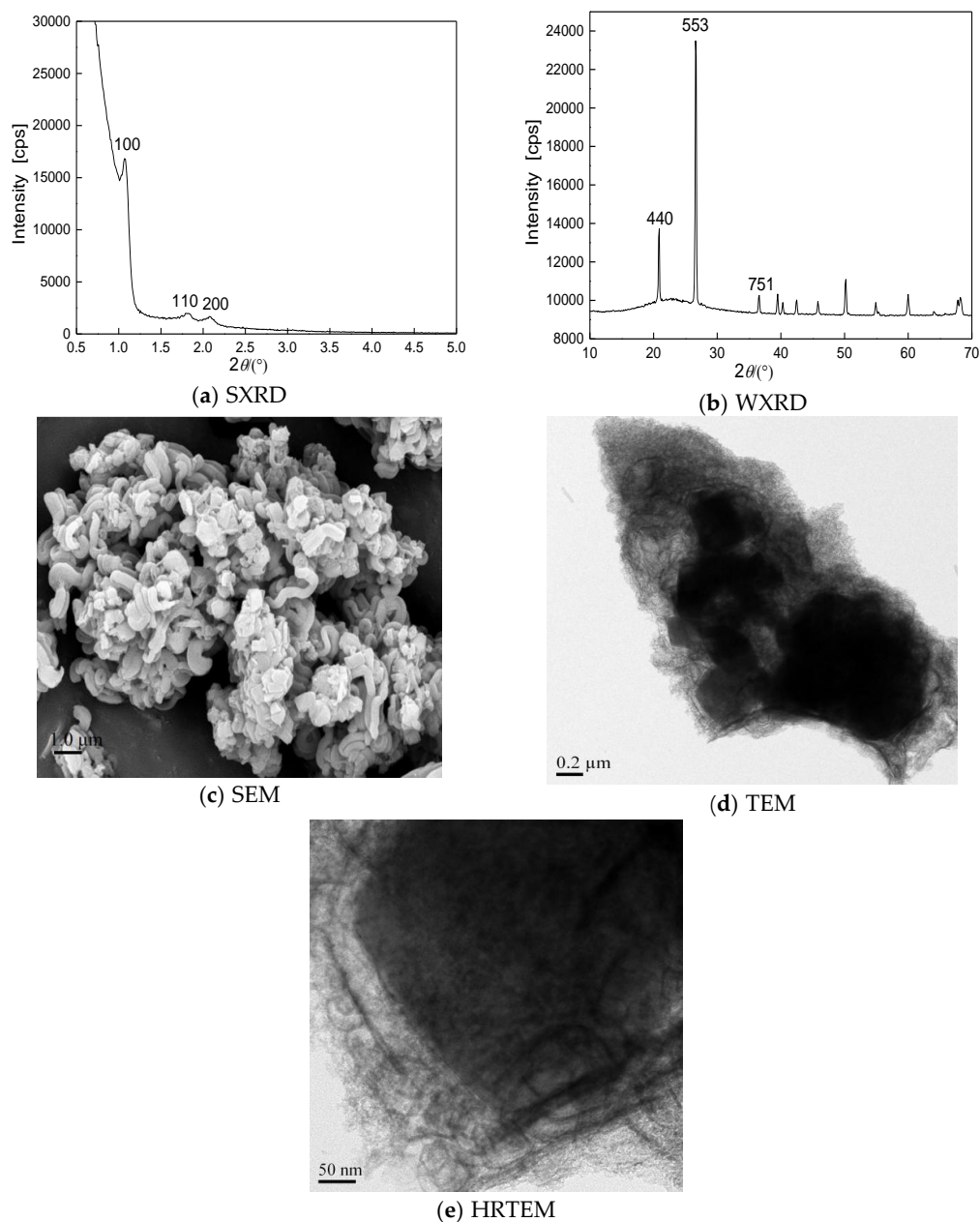


**Figure 1.** X-ray diffraction (XRD), scanning electron microscopy (SEM), transmission electron microscopy (TEM), and HRTEM (High power transmission electron microscopy photos) of YSV.

## 2.2. Characterization of YSG Micro-Mesoporous Composite Molecular Sieve

XRD results of YSG composite molecular sieves are shown in Figure 2a,b, both small angle and wide angle were observed, which are characteristic peaks of mesoporous and microporous, respectively. The SEM result showed they were spherical particles with a slightly rough surface,

a quite uniform size and high surface density, which was consistent with the TEM result (Figure 2d,e). Taken together, YSG micro-mesoporous composite molecular sieve showed Y-type cores and SBA-15 mesoporous shell around the core. However, it showed a Y-type microporous structure, while the shells showed cotton-like SBA-15 mesoporous structure around the cores. This may be contributed to by low nucleation temperature, which can lead to the incomplete growth of the mesoporous.

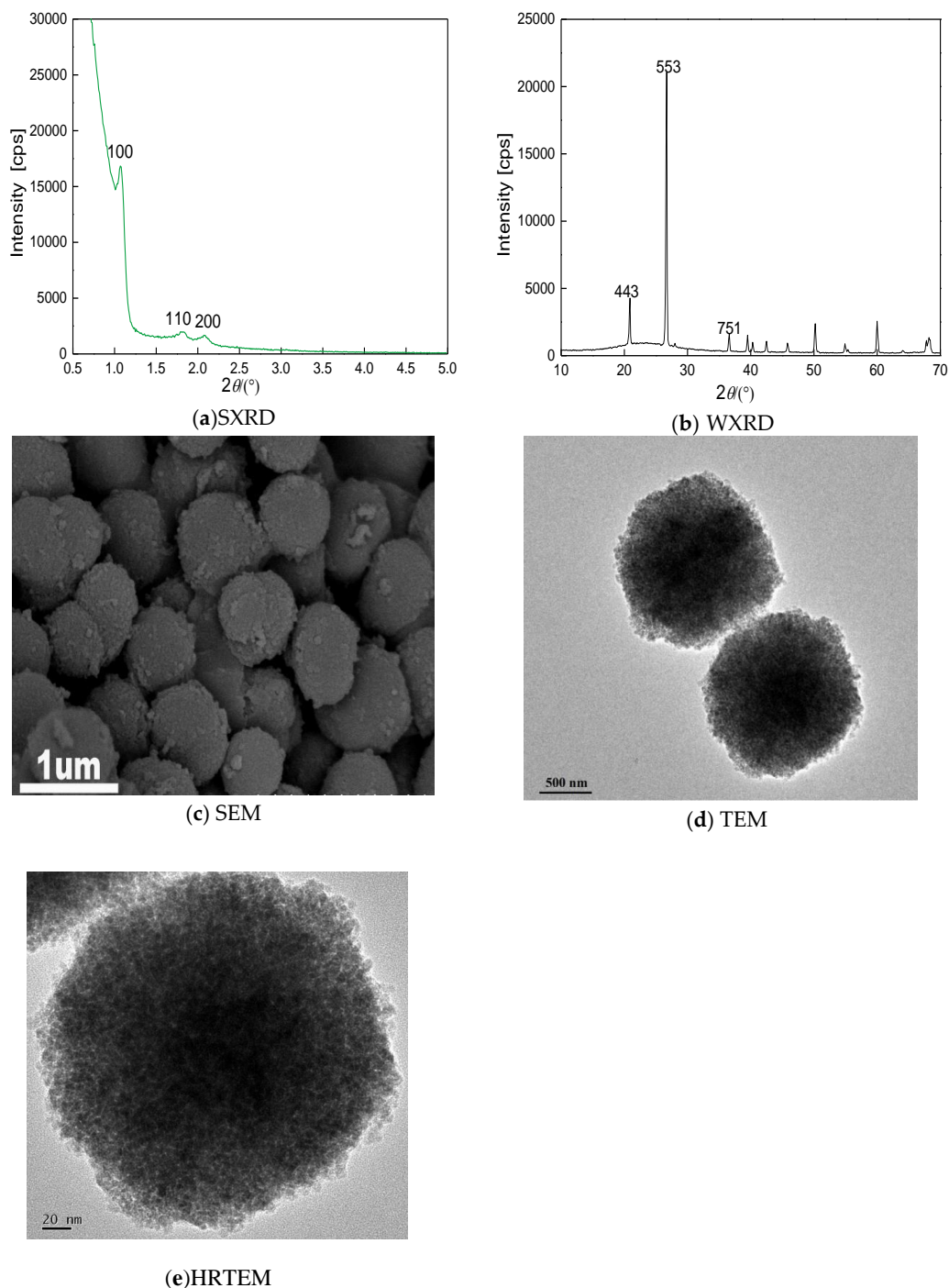


**Figure 2.** XRD, SEM and TEM and HRTEM photos of YSG.

### 2.3. Characterization of YST Micro-Mesoporous Composite Molecular Sieves

As shown in Figure 3, the characteristic peak of SBA-15 was observed (Figure 3a), while the amorphous scattering peaks of SBA-15 and the crystalline scattering peak of Y-type molecular sieve

were clearly observed (Figure 3b), indicating their co-existence. Figure 3c showed that no octagonal crystal grain of single Y-type microporous zeolite was observed, while the particle morphology was also different from that of SBA-15 mesoporous molecular sieve. Their overall shape looked like pipes and was regular, being composed of column-like molecular sieves. These indicated that SBA-15 mesoporous molecular sieves grew along the outer surface of Y-type microporous zeolite. As shown in Figure 3d,e, the mesoporous was in a regular and ordered shape, indicating that the appropriate temperature during the nucleation stage was key to the growth of the mesoporous.

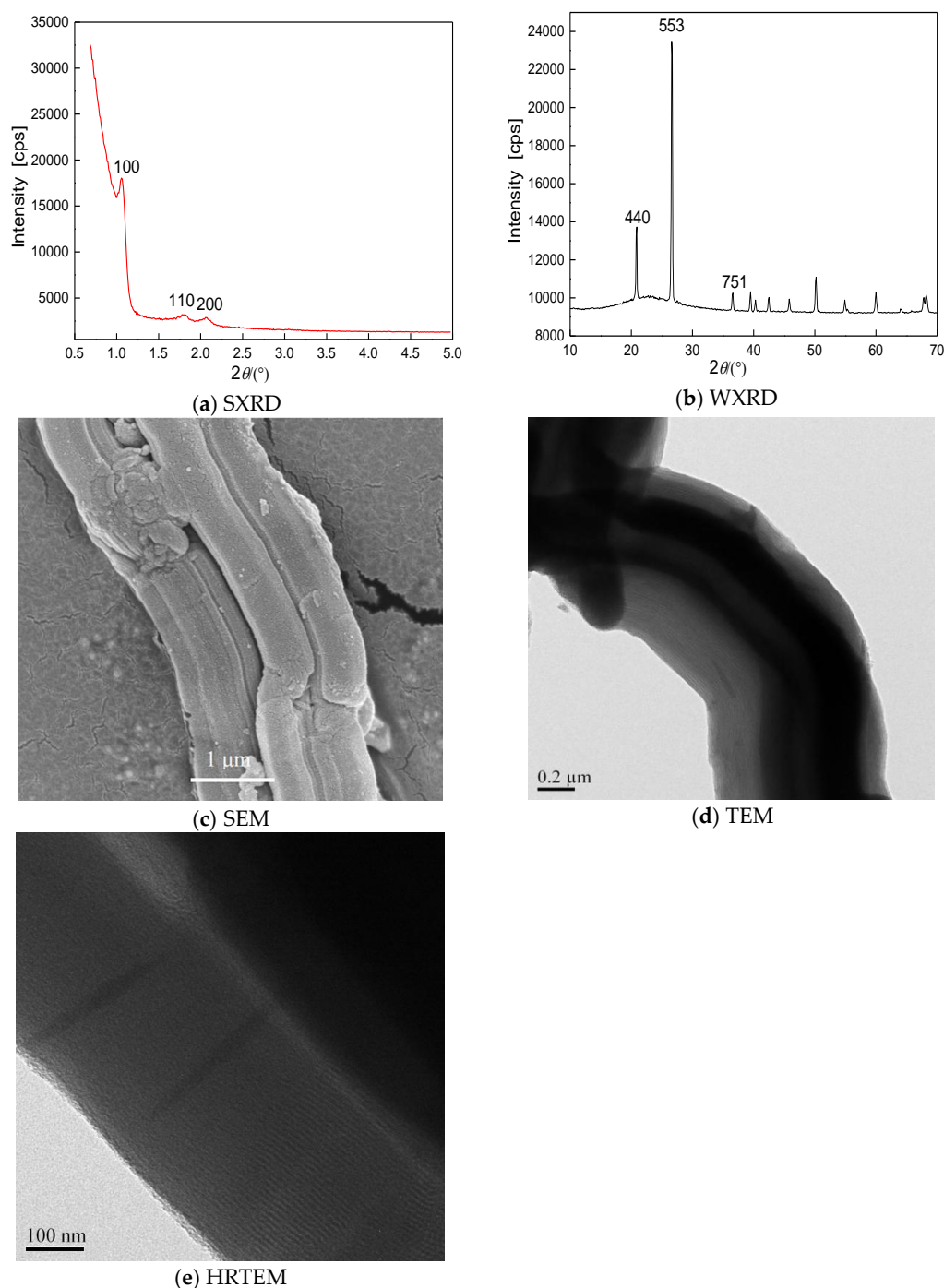


Figure 3. XRD, SEM and TEM and HRTEM photos of YST.

To further confirm the simultaneous presence of microporous and mesoporous structures, the nitrogen adsorption-desorption test was performed for the YST. As shown in Figure 4, the adsorption-desorption isotherms for Y is a typical line, which is the characteristic for microporous molecular sieves, and that for SBA-15 it was a typical line, which is the characteristic for microporous molecular sieves, while that for YST was IV line at a low relative pressure stage, which is characteristic for micro-mesoporous molecular sieves [17].

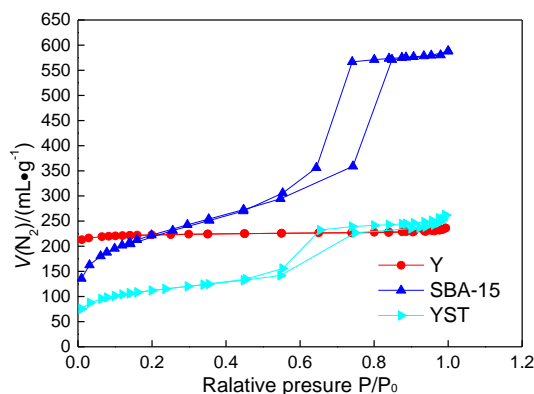


Figure 4.  $N_2$  adsorption-desorption isotherms of Y, SBA-15 and YST.

#### 2.4. Kinetics Analysis of the Synthesis

The crystallization kinetics curves of YST, YSG, and YSV micro-mesoporous composite molecular sieves were first produced at different nucleation temperature but under the same crystallization temperature (373 K). As shown in Figure 5, the relative crystallinity of the YSV composite molecular sieve rose slowly under the same crystallization temperature, while its nucleation induction period was long, and the nucleation rate and growth rate of crystal were also correspondingly slow. With the extension of crystallization time, the relative crystallinity of YSG and YSV molecular sieves increased rapidly in a short time. After a period of crystallization, the crystallization rate slowed down, and declined after reaching their respective peaks.

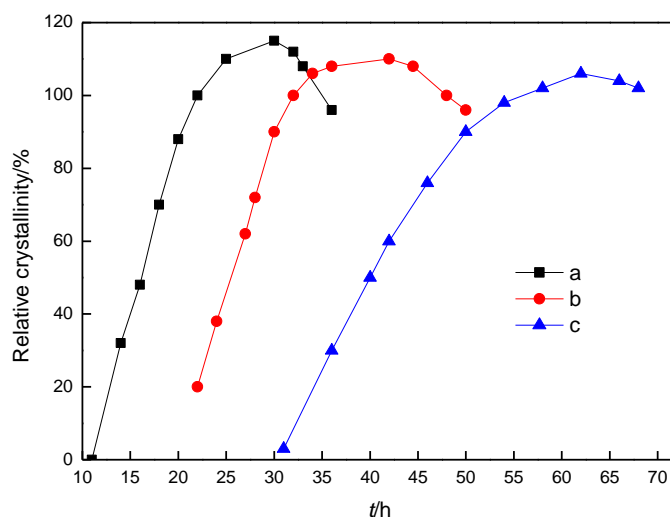


Figure 5. Crystallization fitting curves for synthesis of YST (a), YSG (b), YSV (c) composite molecular sieves at different nucleation stage temperatures.

A computer simulation was also carried out to stimulate the rapid rising section of the crystallization curves according to a previous report, which the curves were extended to zero

crystallinity [17–19]. Obtained data, including the nucleation induction period, apparent nucleation rate, and apparent crystal growth rate, are listed in Table 1. The results showed that with the increase in the nucleation temperature, the nucleation induction period was significantly shortened [20–23], while the nucleation rate was significantly accelerated, and the crystal growth rate was also increased. As compared with crystal growth, nucleation is a slow process. Therefore, when the crystallization temperature and time keep the same, the degree of mesoporous phase crystallization is impaired if the nucleation temperature is low. Therefore, the nucleation temperature plays an important role in the crystallization degree of mesoporous structures of composite molecular sieves.

**Table 1.** Induction period apparent nucleation rate and apparent crystal growth rate during the hydrothermal synthesis of YST, YSG, and YSV composite molecular sieves.

Composite Molecular Sieves	$t_0/h$	$V_n/h^{-1}$	$V_g/h^{-1}$
YST	6.56	0.162	11.87
YSG	11.24	0.097	11.65
YSV	17.86	0.051	10.98

### 2.5. Investigation Their Performance on Isomerization of *N*-Pentane

The prepared YST, YSG, and YSV composite molecular sieves were then investigated as catalysts on isomerization of *n*-pentane, which were compared with the traditional Y-type single molecular sieve without composite porous structure. The reactions were carried out under the conditions in the experimental section, and their performance was summarized in Table 2. The results showed that the isomerization performance of YST, YSG, and YSV composite molecular sieves was significantly higher than that of the traditional Y-type single molecular sieve. The isomerization performance of the composite molecular sieves was more improved than the single molecular sieve, regardless of the regularity of the composite sieve [24]. Moreover, the YSG composite molecular sieve with higher mesoporous regularity than the YSV composite molecular sieve exhibited higher isomerization selectivity than YSV composite molecular sieve, while the YST composite molecular sieve with the best mesoporous channel regularity displayed the best isomerization selectivity among these four molecular sieves, which reached 95.81%. The improved isomerization performance of YST, YSG, YSV composite molecular sieves is mainly due to the introduction of mesoporous, improving the mass transfer efficiency, thus shortening the reaction time of *n*-pentane on the molecular sieves. Thus, it inhibits further decomposition of *n*-pentane on molecular sieves, improving the isomerization selectivity of the reaction. With respect to YST, YSG, and YSV composite molecular sieves, the regularity of mesoporous pores tends to be good to bad due to different nucleation temperatures. Therefore, the mass transfer effect of YSV and YSG composite molecular sieves with more irregular mesoporous is far less than that of the YST composite molecular sieve, thus their isomerization performance is lower than that of YST composite molecular sieve.

**Table 2.** Performance of different catalysts for hydroisomerization.

Item	Catalyst			
	YST	YSG	YSV	Y
<i>n</i> -pentane	37.21	47.86	56.12	70.33
Dimethyl butane	48.43	34.21	24.13	7.82
Naphthenic hydrocarbon	11.36	8.02	7.51	1.81
Hexane	1.48	1.21	0.49	1.09
Others	1.52	8.70	11.75	18.95
Isomerization selectivity/%	95.81	86.23	74.59	61.65

### 3. Experimental

Sodium aluminate, sodium hydroxide, sodium silicate, cerium nitrate, heptanes, toluene and tetraethyl orthosilicate (TEOS) were all analytical pure reagents and purchased from Sinopharm Group Co. LTD. (Shanghai, China) Triblock copolymer poly (ethylene glycol)-block-poly (propylene glycol)-block-poly (ethylene glycol) (Pluronic P123) was purchased from Sigma Aldrich (St. Louis, MA, USA). Y type microporous materials is provided by Fushun Petrochemical Research Institute.

In a three-necked flask, 4.0 g triblock copolymer copolymer P123 was completely dissolved into 30.0 mL water, 9.50 g TEOS was then added and stirred thoroughly. Then 4.0 g of prepared HY was added in the mixtures five times. Next, 120 mL hydrochloric acid at 30% volume fraction was added, respectively, and adding an appropriate amount of water to adjust the solution pH value to 2.5, and the resulting mixture was stirred at 10, 25, 40 °C temperature for 24 h, respectively. The resulting mixture was transferred into a hydrothermal reactor kettle, and placed in an oven under 100 °C, which was used for crystallization for 10–70 h. After the reaction, the reaction solution was taken out and filtered, the products were repeatedly washed with distilled water and ethanol, and then dried under 110 °C. Finally, Y/SBA-15 microporous-mesoporous composite molecular sieves (YSV, YSG, YST) were obtained through calcination at 550 °C for 6 h.

XRD patterns of the catalysts were obtained with an XRD-700 X-ray diffractometer in the 2 theta ranges of 0.5–70° by using Cu K $\alpha$  radiation combined with a Ni filter (Shimadzu Co. Ltd., Tokyo, Japan). Surface morphology of the samples was studied by scanning electron microscopy (SEM) at a magnification of 250,000–1,000,000 microscope (JEOL Co. Ltd., Tokyo, Japan). Transmission electron microscopy (TEM) micrographs were collected on a Philips CM200 microscope (Philips Co. Ltd., Amsterdam, Holland). NH<sub>3</sub>-TPD patterns were recorded on a RC-IR-TP-3030 (Science and Technology Development Co. Ltd., Shanghai, China) to detect surface acidity of the molecular sieves.

The probe reaction was performed on a continuous-flow high-pressure microreactor-chromatography apparatus, which was assembled by our lab. The parameters were set at: 220 °C of reaction temperature, 2 h of reaction time, 8:1 of hydrogen/*n*-pentane ratio, 3 h<sup>-1</sup> of space velocity. The prepared YSV, YSG, and YST served as catalysts to conduct hydroisomerization reaction under these conditions.

### 4. Conclusions

In this work, three core-shell structured microporous-mesoporous composite molecular sieves were synthesized based on the epitaxial growth. They were thoroughly characterized by a range of techniques including SEM, TEM, and XRD, and the results demonstrated that the order of mesoporous regularity of them from good to bad was YST, YSG, and YSV. The effect of the nucleation temperature on the synthesis of composite molecular sieves was also investigated under the same crystallization conditions. The results indicated that with the increase of the nucleation temperature, the nucleation rate was significantly accelerated. Nucleation was a slow process compared with crystal growth. Therefore, lower nucleation temperature impaired the degree of mesoporous phase crystallization, indicating that the nucleation temperature is key to porous structures of composite molecular sieves. Furthermore, employing isomerization of *n*-pentane as a model reaction, their performance was examined. Results showed that the higher nucleation temperature lead to the higher isomerization selectivity of *n*-pentane, indicating that the regularity of the mesoporous structure determines the isomerization selectivity of alkane.

**Author Contributions:** C.S. and W.W. wrote the main manuscript text and J.L., X.B., P.C., Z.Y. and C.L. prepared Figures 1–4. All authors reviewed the manuscript.

**Funding:** This research was funded by [Foundation of Liaoning Province Education Administration] grant number [2017LQN002], [China Scholarship Council] grant number (201908210456), [Natural Science Foundation of Liaoning Province] grant number [2019-ZD-0055], [National Natural Science Foundation of China] grant number [21671092] and [the Liaoning Revitalization Talents Program] grant number [XLYC1802057].

**Conflicts of Interest:** The authors declare no competing both financial and non-financial interests.

## References

1. Kong, D.; Zhang, J.; Yuan, X.; Wang, Y.; Fang, D. Fabrication of core/shell structure via overgrowth of ZSM-5 layers on mordenite crystals. *Microporous Mesoporous Mat.* **2009**, *119*, 91–96. [[CrossRef](#)]
2. Gunst, D.; Alexopoulos, K.; Borght, K.V.D. Study of butanol conversion to butenes over H-ZSM-5: Effect of chemical structure on activity selectivity and reaction pathways. *Appl. Catal. A Gen.* **2017**, *539*, 1–12. [[CrossRef](#)]
3. Zhang, L.; Wang, H.Y.; Jiang, Z.X. Synthesis and catalytic activity of core-shell MFI/CHA zeolites. *Acta Phys. Chim. Sin.* **2016**, *32*, 745–752.
4. Pérez-Romo, P.; Armendáriz-Herrera, H.; Valente, J.S.; de Lourdes Guzmán-Castillo, M.; Hernández-Beltrán, F.; Fripiat, J.J. Crystallization of faujasite Y from seeds dispersed on mesoporous materials. *Microporous Mesoporous Mater.* **2010**, *132*, 363–374. [[CrossRef](#)]
5. Shi, C.W.; Wu, W.Y.; Li, S.; Bian, X.; Zhao, S.L.; Pei, M.Y. Investigation of Y/SBA composite molecular sieves morphology control and catalytic performance for n-Pentane aromatization. *Sci. Rep.* **2016**, *6*, 23826. [[CrossRef](#)]
6. Liu, H.; Li, H.P.; Zhao, H.; Jiao, L. Catalytic acetylation of anisole with Ce- $\beta$ /MCM-41. *J. Liaoning Shihua Univ.* **2018**, *38*, 13–19.
7. Cheng, Y.; Yang, Y.; Luo, G.X. Green synthesis of methyl oleate catalyzed by H3PW12O40/ Y- $\beta$ . *J. Liaoning Shihua Univ.* **2014**, *34*, 11–16.
8. Tian, S.; Li, H.P.; Zhao, H.; Qi, X.Q.; Han, C.; Dong, H.J.; Song, G. Synthesis and characterization of Y/MCM-41 composite molecular sieve. *J. Petrochem. Univ.* **2015**, *28*, 20–25.
9. Wan, H.; Zhao, R.J.; Qi, Y.C.; Lu, C.T.; Zhang, X.T.; Song, L.J. Morphology control and aromatization of ZSM-5/KL composite zeolite. *J. Petrochem. Univ.* **2015**, *28*, 1–7.
10. Du, J.L.; Shi, C.W.; Wu, W.Y.; Bian, X.; Chen, P.; Cui, Q.Z.; Cui, Z.X. Synthesis of core-shell structured FAU/SBA-15 composite molecular sieves and their performance in catalytic cracking of polystyrene. *Sci. Technol. Adv. Mater.* **2017**, *18*, 939–949. [[CrossRef](#)]
11. Yamamoto, E.; Kuroda, K. Colloidal mesoporous silica nanoparticles. *Bull. Chem. Soc. Jpn.* **2016**, *89*, 501–539. [[CrossRef](#)]
12. Dutta, S.; Bhaumik, A.; Wu, K.C.W. Hierarchically porous carbon derived from polymers and biomass: Effect of interconnected pores on ene.g., applications. *Ene.g., Environ. Sci.* **2014**, *7*, 3574–3592. [[CrossRef](#)]
13. Malgras, V.; Ataee-Esfahani, H.; Wang, H.J.; Jiang, B.; Li, C.L.; Wu, K.C.W.; Kim, J.H.; Yamauchi, Y. Nanoarchitectures for mesoporous metals. *Adv. Mater.* **2016**, *28*, 993–1010. [[CrossRef](#)] [[PubMed](#)]
14. Yang, D.H.; Shi, B.B.; Wang, X.B.; Wu, Z.H.; Liu, X.; Dou, T. Hydrothermal crystallization kinetics of EU-1 zeolite containing iron series of elements. *Chem. J. Chin. Univ.* **2013**, *10*, 2363–2369.
15. Xing, A.H.; Feng, Q.Y.; Zhang, X.F.; Jiang, J.D. Development in crystallization mechanism and crystallization kinetics of SAPO-34 molecular sieves. *Ind. Catal.* **2016**, *24*, 5–13.
16. Hammed, A.K.; Dewayanto, N.; Du, D. Novel modified ZSM-5 as an efficient adsorbent for methylene blue removal. *J. Environ. Chem. Eng.* **2016**, *4*, 2607–2616. [[CrossRef](#)]
17. Fa-Kuen, S.; Wang, S.C.; Yen, C.-I.; Wu, C.C.; Dutta, S.; Chou, L.Y.; Morabito, J.V.; Hu, P.; Hsu, M.H.; Wu, K.C.W.; et al. Imparting functionality to biocatalysts via embedding enzymes into nanoporous materials by a de novo approach: Size-selective sheltering of catalase in metal-organic framework microcrystals. *J. Am. Chem. Soc.* **2015**, *137*, 4276–4279.
18. Ren, Y.Q.; Liu, B.Y.; Kiryutina, T.; Xi, H.X.; Qian, Y. Investigation of structure formation mechanism of a mesoporous ZSM-5 zeolite by mesoscopic simulation. *Chem. Phys.* **2015**, *448*, 9–14. [[CrossRef](#)]
19. Chen, H.Y.; Xi, H.X.; Cai, X.Y.; Qian, Y. Experimental and molecular simulation studies of a ZSM-5-MCM-41 micro-mesoporous molecular sieve. *Microporous Mesoporous Mater.* **2009**, *118*, 396–402.
20. Ariga, K.; Yamauchi, Y.; Rydzek, G.; Ji, Q.M.; Yonamine, Y.; Wu, K.C.W.; Hill, J.P. Layer-by-layer nanoarchitectonics: Invention, innovation, and evolution. *Chem. Lett.* **2014**, *43*, 36–48. [[CrossRef](#)]
21. Grandjean, D.; Beale, A.M.; Petukhov, A.V.; Weckhuysen, B.M. Unraveling the crystallization mechanism of CoAPO-5 molecular sieves under hydrothermal conditions. *J. Am. Chem. Soc.* **2005**, *127*, 14454–14465. [[CrossRef](#)] [[PubMed](#)]

22. Selvam, P.; Mohapatra, S.K. Synthesis and characterization of divalent cobalt-substituted mesoporous aluminophosphate molecular sieves and their application as novel heterogeneous catalysts for the oxidation of cycloalkanes. *J. Catal.* **2005**, *233*, 276–287. [[CrossRef](#)]
23. Depla, A.; Lesthaeghe, D.; Svan, E.T.; Aerts, A.; Houthoofd, K. <sup>29</sup>Si NMR and UV–Raman investigation of initial oligomerization reaction pathways in acid-catalyzed silica sol–gel chemistry. *J. Phys. Chem. C* **2011**, *115*, 3562–3571. [[CrossRef](#)]
24. Zhang, J.T.; Song, J.; Zhen, X.; Shen, Z.B.; Liang, S.R. Synthesis of MCM-41/MOR composite molecular sieves and its catalytic properties for isomerization of alkane. *J. Fuel Chem. Technol.* **2017**, *45*, 676–681.



© 2019 by the authors. Licensee MDPI, Basel, Switzerland. This article is an open access article distributed under the terms and conditions of the Creative Commons Attribution (CC BY) license (<http://creativecommons.org/licenses/by/4.0/>).